Optoelectronic Fibers via Selective Amplification of In-Fiber Capillary Instabilities

*Lei Wei, Chong Hou, Etgar Levy, Guillaume Lestoquoy, Alexander Gumennik, Ayman F. Abouraddy, John D. Joannopoulos, and Yoel Fink**

Recent advances in fiber material processing have enabled the realization of optoelectronic devices within fibers, opening the path toward large-area, flexible device architectures that can be incorporated into fabrics. A number of approaches have been developed to realize in-fiber optoelectronic devices. One of them is based on prefabricated hollow fibers, which are used as a substrate for the subsequent infiltration or deposition of semiconductor material on their internal surface.[1–6] Another approach is based on the well-established fiber drawing techniques, in which a macroscopic version of the targeted multimaterial micro- or nanostructure containing all of the desired materials is fabricated and subsequently thermally drawn and scaled down to the desired dimensions.[7–14] The incorporation of a range of co-drawable glassy semiconductors, metals, and polymers has led to the fabrication of a rich variety of fibers with functionalities spanning from optics to optoelectronics, albeit limited in their performance due to the amorphous nature of the semiconducting materials employed.[15,16] Introducing high temperature crystalline semiconductors such as silicon (Si) or germanium (Ge) into silica fiber materials presents new hypothetical possibilities for improving the performance of in-fiber semiconductor devices while harnessing the intrinsic scalability of the fiber drawing process.[17–21] However, to draw such fiber devices one needs to overcome what at first seems like a fundamental barrier: thermal co-drawing of crystalline semiconductors and metallic domains requires their melting, which in turn leads to mixing and a disruption of the device structure. Even if the adjacent melted semiconductor–metal domains did not mix, the diffusion at elevated temperatures would result in significant doping of the semiconductor domain hence significantly altering its properties.

In this study, we introduce the first fully functional optoelectronic in-silica fiber device using high temperature semiconductors in a precisely defined metal–semiconductor–metal device architecture. To achieve these results, a process involving two key steps was developed: First a silica fiber containing three internal spatially separated cylindrical domains, a central semiconductor flanked with two metal cylinders, was thermally drawn from a macroscopic preform. In this step a wide enough silica barrier is maintained all the time during the thermal draw in order to prevent different domains contacting and mixing. After the draw, the fiber was then heated so that the semiconductor cylindrical domain undergoes a Rayleigh–Plateau instability,[22–26] and transform to spheres of larger diameter that bridge the gap between the conductors, and thus create an electrical connection. We especially choose the materials with distinct melting points as well as the breakup s so that only one domain experiences the fluid instability while the other is not impacted. This step, in which the semiconducting core is selectively broken up into a series of relatively larger spheres, results in direct contacts between semiconducting spheres and the two continuous metal filaments. The ladder-like final structure not only forms an integrated device in a single silica fiber that exhibits measurable photosensitive properties, but also dramatically increases the density of functional components over the entire fiber length when compared to previously achieved continuous-core photosensitive fibers. The high quality in-fiber optoelectronic device can be potentially applied in a wide range of areas, such as wearable devices, imaging and diagnostic technologies, geophysical exploration, and national security.

We begin our process by constructing a macroscopic version of the desired structure (the "preform") using custom-developed

Prof. L. Wei
School of Electrical and Electronic Engineering
Nanyang Technological University
50 Nanyang Avenue 639798, Singapore
Dr. C. Hou, Dr. E. Levy, Dr. G. Lestoquoy,
Prof. J. D. Joannopoulos, Prof. Y. Fink
Research Laboratory of Electronics
Massachusetts Institute of Technology
Cambridge, MA 02139, USA
E-mail: yoel@mit.edu
Dr. C. Hou, Prof. Y. Fink
Department of Materials Science and Engineering
Massachusetts Institute of Technology
Cambridge, MA 02139, USA
Dr. C. Hou, Prof. J. D. Joannopoulos, Prof. Y. Fink
Institute for Soldier Nanotechnology
Massachusetts Institute of Technology
Cambridge, MA 02139, USA
Prof. A. Gumennik
Department of Intelligent Systems Engineering
Indiana University Bloomington
Bloomington, IN 47408-2664, USA
Prof. A. F. Abouraddy
CREOL
The College of Optics & Photonics
University of Central Florida
Orlando, FL 32816, USA
Prof. J. D. Joannopoulos
Department of Physics
Massachusetts Institute of Technology
Cambridge, MA 02139, USA
Prof. Y. Fink
Department of Electrical Engineering and Computer Science
Massachusetts Institute of Technology
MA 02139, USA

DOI: 10.1002/adma.201603033

glass processing technique and the preform is subsequently scaled down to microscopic dimensions via thermal drawing. The preform is composed of fused silica (as cladding) and three different cores. The middle core is a germanium rod and the other two are platinum rods. All the semiconductor and metal cores are surrounded and hence separated by the silica tubes. The top-left of **Figure 1**a schematically illustrates this step as well as the cross-sectional structure and the composition of the preform. As previously mentioned, the choice of materials is paramount in the success of both the initial thermal-drawing and the subsequent controlled capillary breakup steps. Since the latter naturally calls for the use of a high melting temperature of the metal domains, we choose platinum (Pt) (melting point: 1768 °C) as electrode material. Similarly, in order to maximize the difference in melting temperature between metallic and semiconducting domains, we favor doped Ge (melting point: 938 °C) as semiconducting core material over Si (melting point: 1414 °C). Moreover, doped Ge has a smaller bandgap, greater near-infrared quantum efficiency, and higher carrier mobility than Si.[27] A triple-core preform which contains two Pt 1 mm diameter rods flanking a central Ge 0.8 mm diameter rod is fabricated. Both Pt and Ge are crystalline materials, exhibiting low viscosities and high diffusivities when molten during the thermal drawing. These characteristics would lead to an uncontrollable interdomain mixing and diffusion if Pt and Ge were to be or come in contact with each other during the drawing process.[28] To keep the constituent materials separated at all times, a viscous silica barrier is intentionally placed between the cores of this two-material triple-core structure at the preform level by confining all the rods in separate silica tubes, which are arranged in a row with 1 mm wide separations as illustrated in Figure 1a. To ensure proper structural support during the draw, the preform is further cladded with concentric silica tubes to thicken the cladding up to a total outer diameter of 15 mm. Any empty space inside the preform is filled up with thin silica rods, and the entire assembly is sealed from both ends under vacuum to prevent oxidation of functional materials during the drawing process. The challenge of drawing such a structure lies in maintaining the integrity and symmetrical arrangement of the multiple cores down to the final scale while preventing the deformation caused by fluidic instabilities that can occur when the silica cladding is too soft and the Pt and Ge cores are in liquid phase. To prevent that, the preform is loaded in a fiber draw tower and thermally drawn into a fiber at the relatively low temperature of 2000 °C, at which the silica remains viscous enough to provide a structural support to the liquid cores. The optical microscope image in Figure 1b depicts the cross section of the resulting fiber structure, where the Ge core in the center is surrounded by two Pt electrodes with silica barriers in between. The diameters of Ge core and Pt electrodes are scaled down to about 40 and 50 µm, respectively.

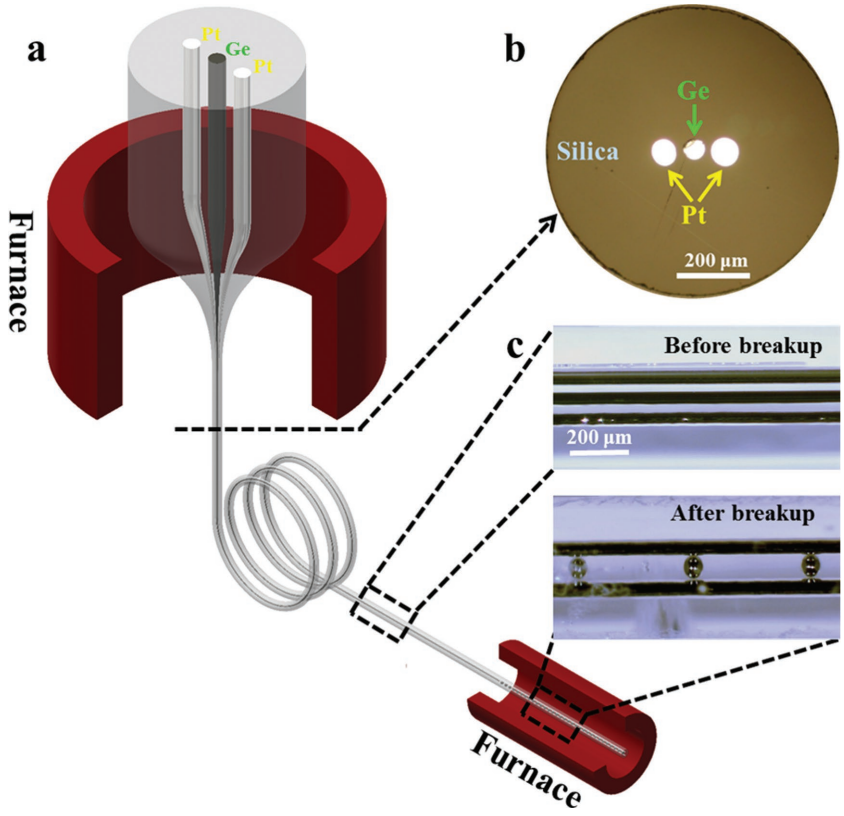

Figure 1. a) Schematic representation of the thermal drawing of a triple-core fiber and post-draw selective breakup process in a heating furnace. b) Optical microscope image of the obtained fiber cross section. The resulting silica-cladding fiber contains one central semiconductor (germanium) core flanked by two metal (platinum) cores. c) Side views of the triple-core fiber before and after the selective breakup process.

Following the draw, the resulting fiber is heated to selectively induce the PRI of the semiconductor region along the entire fiber length while keeping the metal wires intact. At elevated temperature, an axially uniform viscosity reduction along the fiber length provokes the breakup of the cylindrical core into discrete spheres as a result of the core-cladding boundary minimizing its interfacial energy. While instabilities occur at all wavelengths shorter than the total length of fiber being processed, the break-up of the continuous semiconductor core yields a periodic structure of discrete spheres, because a specific wavelength maximizes the instability growth rate and thus kinetically dominates all others. This dominant periodicity, and thus the size of the produced spheres is dictated by the core diameter and its viscosity contrast relative to the silica cladding. As indicated previously, the former is adjustable during the draw, while the latter is a direct function of the temperature later applied. To break up the Ge core into spheres while leaving the Pt electrodes intact, this temperature should satisfy the following conditions: (1) it should be higher than the melting point of Ge to initialize the fluid instability, (2) it should be above the silica glass softening temperature of 1683 °C to decrease the viscosity contrast

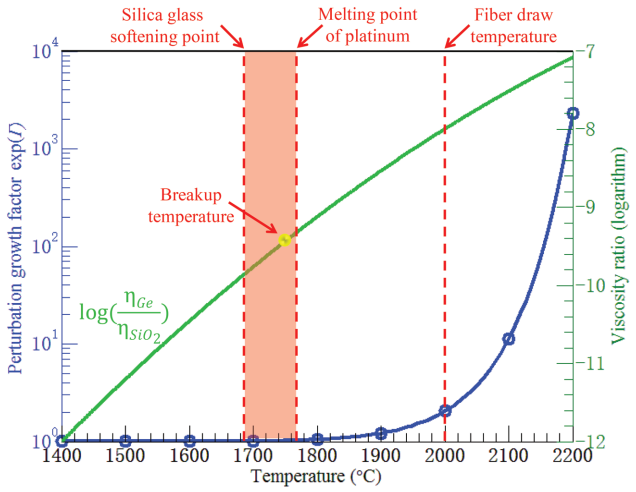

Figure 2. Viscosity contrast of Ge/SiO_2 (green curve) and perturbation growth factor, exp(Γ) (blue curve with calculated points marked by blue circles) as a function of temperature. All the processing temperatures are indicated, including fiber draw temperature of 2000 °C, breakup temperature of 1750 °C, silica glass softening temperature of 1683 °C, and Pt melting point of 1768 °C.

between Ge and silica enough to induce perturbations with reasonably fast growth rate, and 3) it should be lower than the Pt melting point to preserve the fixed wire shape of the Pt electrode. All the relevant temperatures are indicated in **Figure 2**, where the breakup temperature range satisfying the conditions above is indicated by the red-shaded region. In practice, after drawing, a 10 cm long section of fiber is kept inside a furnace for 40 min at a constant temperature of 1750 °C. In these conditions, the Ge core is in its liquid state and the silica cladding is at a low achievable viscosity without melting the Pt electrodes. Only the Ge core is thus influenced by the fluid instability and breaks up into a chain of Ge spheres with a diameter of ≈110 µm, while the Pt electrodes remain unperturbed. The sphere diameter D_s is always larger than the diameter of the core from which it breaks D_c ($D_s = (3/2PD_c^2)^{1/3}$, where P is the particle spacing, and according to the Rayleigh condition $P > \text{pi}*D_c$),[25,26] therefore the PRI-induced Ge spheres push the silica barriers aside and come in contact with the two solid Pt electrode wires, forming a ladder-like structure. The side view images of the fibers before and after the selective breakup process are shown in Figure 1c. This directed physical self-assembly process breaks the axial-lyinvariant topological structure inside the fiber and allows the simultaneous formation of periodically-spaced, discrete in-fiber electrical contact between crystalline semiconductor and metal materials, leading to an integrated optoelectronic multisensory device within the silica fiber. Additionally, the density of in-fiber integrated components per unit length is dramatically increased by this selective breakup process, in which a single cylindrical device turns into a multitude of electrically addressable spherical devices linearly frozen in place within the silica cladding. The density can be further increased either by reducing the size of triple-core structure or by integrating multiple groups of triple-core structure within a single fiber.

A capillary breakup is expected when a perturbation starts to grow such that its amplitude becomes comparable with the correspondent fiber diameter. Different wavelengths of perturbations grow at different rates. To estimate the perturbation amplitude growth factor of the Ge core in a silica cladding, we consider a perturbation with wavelength of λ and use the Tomotika model that considers two infinite concentric cylinders to calculate the growth rate of the amplitude perturbation (see Supporting Information).[29] Figure 2 describes the viscosity contrast of Ge/SiO_2 (green curve) as a function of temperature,[30–32] and the dependence of the calculated perturbation growth factor on the furnace temperature for a perturbation wavelength of λ = 1 cm. The loading and the drawing speeds in the calculation are set similar to their experimental values: 2 mm min^{-1} and 900 mm min^{-1}, respectively. The theoretical results are consistent with our observations that capillary breakup can be avoided during the draw, while selective breakup of Ge core during the reheating process remains possible with sufficient processing time, since the perturbation wavelength with the fastest growth rates sets the observed breakup period (see Supporting Information).

Beyond its simple visual observation, the realization of in-fiber direct contact between crystalline semiconductor and metal electrodes is further confirmed by applying a bias voltage across the two Pt electrodes of a section of fiber. Before the selective process, the current response is imperceptible at this microampere scale (**Figure 3**a), which proves that the created circuit is open, as expected. After the selective breakup process, measurable current is induced by the applied voltage, and the nearly linear relationship indicates that contacts between Ge spheres and Pt electrode wires are Ohmic. The in-fiber electrode scheme achieved here allows for robust electrical contacts with external circuits on either the end-facets or the side of fiber, and thus no further metal deposition process is required.

As a photosensitive element, the Ge rod used in the preform is n-type with a doping concentration on the order of 10^{17} cm^{-3}. To investigate the optoelectronic performance in the resulting fiber configuration, a 1550 nm laser diode with a maximum output power of 130 mW is used to illuminate the Ge spheres (see Experimental Section). The Pt electrodes which interface with Ge spheres along the entire fiber length are connected to an external circuit. The Ge spheres undergo a change in electrical conductivity when externally illuminated, and a change in slope of the current–voltage (I–V) curve is obtained with respect to dark conditions (Figure 3a).[33] It is noted that the contrast between the dark current and the photocurrent is not high, and the possible reason is that the Ge is heavily doped to form a good Ohmic contact with the Pt wire. Lowering the doping concentration of Ge will result in a rectifying junction between the Ge spheres and the Pt wire but will improve the device optical sensitivity. The ladder-like structure in the fiber together with the photosensitive spheres makes monitoring the illuminated sphere position possible and could finally lead to a distributed sensor array in the future.[34] The electrical bandwidth of the resulting fiber is measured to be 470 kHz under a driving voltage of 3 V by modulating the input 1550 nm laser (Figure 3b), which is three orders of magnitude higher than previously reported fiber-integrated optoelectronic devices made using glassy semiconductors.[7] The measured rise time is on the order of microseconds, as illustrated in the inset of Figure 3b. High-performance optoelectronic devices require

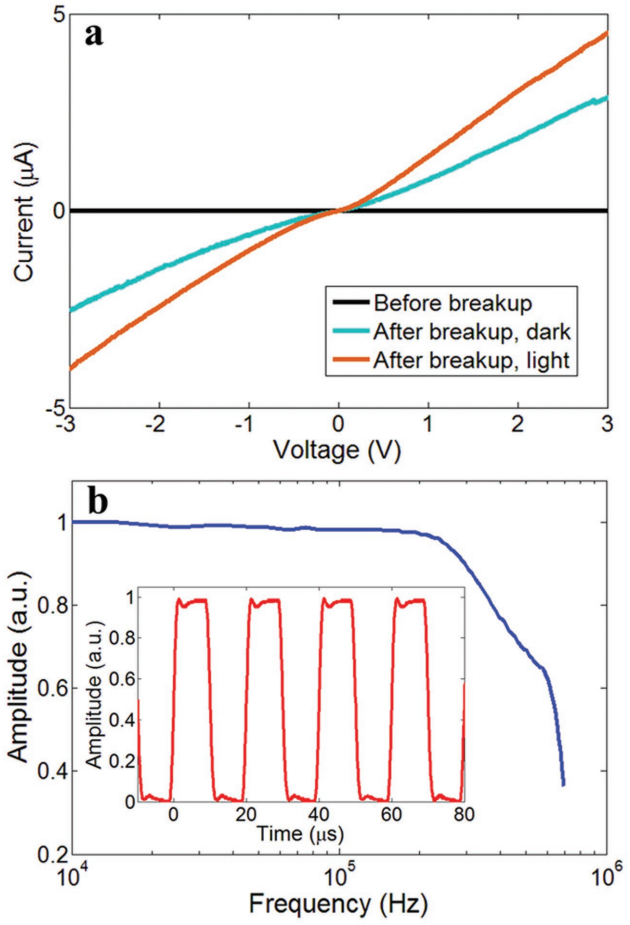

Figure 3. a) Photoconductance of a triple-core fiber before and after the selective breakup process in the dark and on the illumination of a 1550 nm laser. b) Bandwidth of the detector is measured to be 470 kHz. Inset: response time measurement of the resulting fiber on the illumination of a modulated 1550 nm laser.

high-quality semiconductors as the functional materials and junctions as the fundamental components. Therefore, further development in the in-fiber material processing and the realization of in-fiber junction is expected to lead to improvements in device performance. For example, with the recent demonstration of the formation of rectifying p–n junctions in silicon-in-silica fibers by high-pressure chemical vapor deposition, bandwidth of up to 3 GHz and rise time of picoseconds can be achieved.[2] Moreover, changing the composition of the semiconductor core can adjust the spectral characteristics of the photoconductive response.[35,36] For instance, the realization of Si–Ge heterojunction can significantly improve the efficiency and speed of in-fiber-integrated optoelectronic devices.

We further study the dependence of the device performance on the sphere diameter. To generate Ge spheres with smaller diameters, we first reduce the fiber sizes using a high-tension low-downscaling ratio process to prevent any unwanted fluidic instabilities (see Experimental Section). We repeat the process twice, and the resulting diameters of Ge core after the first and second tapering steps are about 18 and 8 μm, as the side views shown in **Figure 4**a,b, respectively. The same selective breakup approach is then applied separately to the resulting fibers, leading to the formation of smaller Ge spheres connected with Pt electrodes, as illustrated in Figure 4a,b. The breakup temperature is maintained at 1750 °C, and the breakup time is shortened in both cases due to the reduced sizes of Ge cores. The diameters of the resulting Ge spheres in fibers after one and two tapering operations are around 48 μm and 21 μm, respectively, which are further confirmed by releasing spheres from the silica fibers using hydrofluoric acid and analyzing dimensions using a scanning electron microscope. The device performance of the resulting fibers with different sphere sizes is then characterized with an illumination of a 1550 nm laser and a 1310 nm laser, as illustrated in Figure 4c. Higher photosensitivity is observed at 1550 nm, which is due to the fact that the photoresponsivity of Ge at 1550 nm is higher than that at 1310 nm.[28] Here, the dark current I_{dark} is defined as the average current in the fiber when no illumination is applied, and the photocurrent I_{light} is the average current under predefined illumination conditions. $I_{light}-I_{dark}$ is inversely proportional to D_s^2 for fixed number of incident photons at a given wavelength, which is limited to the penetration depth of the incident wavelength.[37,38] The dependence of the photoconductance on the sphere size reveals that reducing the sizes of photoconducting Ge spheres can be an efficient way to enhance their photosensitivity. Moreover, smaller-diameter fibers have increased mechanical flexibility, reduced weight and cost, and thus better allow the making of wearable and conformal smart fabrics.

Further improvement in process development and material quality is expected to achieve better device performance and broader functionalities. For example, the isothermal capillary breakup used here is known to frequently induce chaotic regimes where small "satellite" spheres, which do not contact metal electrodes are formed.[22,39] To avoid chaotic regimes, a gradual liquefaction by feeding the fiber into a fixed heating source can be used to induce the formation of monodisperse spheres. A laser as a localized heating source also offers better control of processing temperature and accelerates the breakup process. Moreover, traces of oxygen in the semiconductor core due to the dissolution of the cladding glass in the molten core during the fiber draw process limits the electrical properties of resulting devices. Including an in situ reactive getter of oxygen in the fiber draw process is an effective method to achieve oxygen-free semiconductor core.[40,41] Last but not least, process induced stresses can modify the electronic band structure of the semiconductor material, which allows the fine engineering of optical detection range.[4,42,43] In general, since this fabrication approach relies on a physical breakup mechanism as opposed to chemical synthesis, it significantly broadens the repertoire of usable materials and geometries. In fact, the proposed fabrication process is highly versatile, allowing a variety of families of semiconductors that are sensitive to other physical parameters to be integrated in a single fiber, for example, an energy-harvesting fiber could be realized with the integration of thermoelectric core made by SiGe compound. The interplay between materials properties and structure integration in these fibers opens up opportunities for novel semiconductor device functionalities at fiber-optic length scales, uniformity and cost, leading to the realization of more

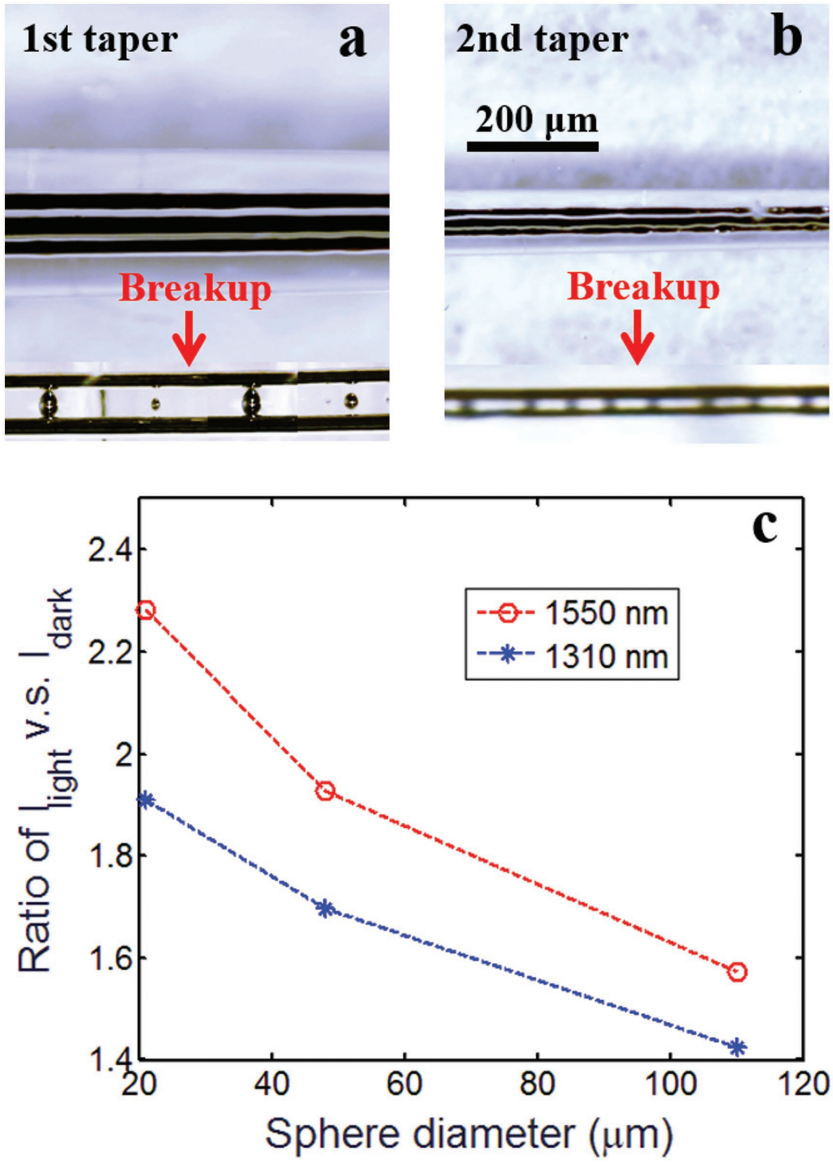

Figure 4. a,b) Side view of triple-core fibers before and after the selective breakup process after first and second tapering process using high-tension low-ratio downscaling method by a hydrogen torch. c) Photoconductance of the resulting fibers with different sphere sizes on the illumination of a 1550 nm laser and a 1310 nm laser.

sophisticated functionalities and the prospect of truly multi-functional fibers.

Experimental Section

Perturbation Amplitude Growth Factor: The growth rate, according to the Tomotika model, was a function of the viscosity ratio between Ge and silica, and of the Ge core diameter D_c. Both the viscosity ratio and the fiber core diameter varied significantly within the furnace heating zone: due to the drawing tension and the high temperature the preform was deformed into a thin fiber and a "neck-down" shape was formed. As a result, the perturbation growth rate varied accordingly along the heating zone. By integrating the perturbation growth rate over the time the perturbation spent in the heating zone, the ratio between the final and the initial perturbation amplitudes, which was defined here as the perturbation growth factor, could be calculated.

Measurement of the Optoelectrical Response of the Fiber: The laser beam was modulated and coupled into the in-fiber Ge sphere through a focal lens. A small fraction of the beam was diverted with a beam splitter to monitor the input power using a power meter (Thorlabs, S122C). Two tungsten needles (Cascade Microtech, PTT-24-25) were brought in contact with the in-fiber Pt electrodes exposed on both end-facets of the resulting optoelectronic fiber using manual probe positioners (Cascade Microtech). Voltage was applied between the probes by a Keithley 6517A Electrometer while current was measured by a Keithley 6487 Picoammeter, and both units were controlled via a LabView custom interface (see Supporting Information).

High-Tension Low-Downscaling Ratio Process: An initial fiber with the same dimensions as the one shown in Figure 1a was chosen, which had a 40 μm diameter Ge core and two 50 μm diameter Pt wires. The downscaling process started with a slow feeding speed of 3 mm min^{-1} and a relatively fast drawing speed of 15 mm min^{-1} under high tension in a hydrogen flame. A scaling factor of $\sqrt{5}$ was therefore obtained.

Supporting Information

Supporting Information is available from the Wiley Online Library or from the author.

Acknowledgements

The authors are grateful to A. M. Stolyarov for fruitful discussions. This work was supported in part by the MIT MRSEC through the MRSEC Program of the National Science Foundation under award number DMR-0819762, the U. S. Army Research Laboratory and the U. S. Army Research Office through the Institute for Soldier Nanotechnologies under contract number W911NF-13-D-0001. This work was also supported in part by the Singapore Ministry of Education Academic Research Fund Tier 2 (MOE2015-T2-1-066) and Nanyang Technological University (Start-up grant: L.W.).

Received: June 8, 2016
Revised: September 12, 2016
Published online: October 31, 2016

[1] P. J. A. Sazio, A. Amezcua-Correa, C. E. Finlayson, J. R. Hayes, T. J. Scheidemantel, N. F. Baril, B. R. Jackson, D. Won, F. Zhang, E. R. Margine, V. Gopalan, V. H. Crespi, J. V. Badding, *Science* **2006**, *311*, 1583.
[2] R. He, P. J. A. Sazio, A. C. Peacock, N. Healy, J. R. Sparks, M. Krishnamurthi, V. Gopalan, J. V. Badding, *Nat. Photonics* **2012**, *6*, 174.
[3] A. C. Peacock, J. R. Sparks, N. Healy, *Laser Photonics Rev.* **2014**, *8*, 53.

[4] N. Healy, S. Mailis, N. M. Bulgakova, P. J. A. Sazio, T. D. Day, J. R. Sparks, H. Y. Cheng, J. V. Badding, A. C. Peacock, *Nat. Mater.* **2014**, *13*, 1122.
[5] H. K. Tyagi, M. A. Schmidt, L. Prill Sempere, P. St. J. Russell, *Opt. Express* **2008**, *16*, 17227.
[6] L. Wei, T. T. Alkeskjold, A. Bjarklev, *Appl. Phys. Lett.* **2010**, *96*, 241104.
[7] M. Bayindir, F. Sorin, A. F. Abouraddy, J. F. Viens, S. D. Hart, J. D. Joannopoulos, Y. Fink, *Nature* **2004**, *431*, 826.
[8] A. M. Stolyarov, L. Wei, O. Shapira, F. Sorin, S. L. Chua, J. D. Joannopoulos, Y. Fink, *Nat. Photonics* **2012**, *6*, 229.
[9] M. Yaman, T. Khudiyev, E. Ozgur, M. Kanik, O. Aktas, E. O. Ozgur, H. Deniz, E. Korkut, M. Bayindir, *Nat. Mater.* **2011**, *10*, 494.
[10] J. Ballato, T. Hawkins, P. Foy, R. Stolen, B. Kokuoz, M. Ellison, C. McMillen, J. Reppert, A. M. Rao, M. Daw, S. Sharma, R. Shori, O. Stafsudd, R. R. Rice, D. R. Powers, *Opt. Express* **2008**, *16*, 18675.
[11] P. Dragic, T. Hawkins, P. Foy, S. Morris, J. Ballato, *Nat. Photonics* **2012**, *6*, 627.
[12] B. L. Scott, K. Wang, G. Pickrell, *IEEE Photonics Technol. Lett.* **2009**, *21*, 1798.
[13] H. K. Tyagi, H. W. Lee, P. Uebel, M. A. Schmidt, N. Joly, M. Scharrer, P. St. J. Russell, *Opt. Lett.* **2010**, *35*, 2573.
[14] A. Tuniz, K. Kaltenecker, B. Fischer, M. Walther, A. Fleming, A. Argyros, B. Kuhlmey, *Nat. Commun.* **2013**, *4*, 2706.
[15] Z. U. Borisova, *Glassy Semiconductors*, Plenum, New York **1981**.
[16] A. K. Varshneya, *Fundamentals of Inorganic Glasses*, Academic, New York **1994**.
[17] R. Davis, R. Rice, A. Ballato, T. Hawkins, P. Foy, J. Ballato, *Appl. Opt.* **2010**, *49*, 5163.
[18] J. Ballato, T. Hawkins, P. Foy, S. Morris, N. K. Hon, B. Jalali, R. Rice, *Opt. Lett.* **2011**, *36*, 687.
[19] F. A. Martinsen, J. Ballato, T. Hawkins, U. J. Gibson, *Appl. Phys. Lett. Mater.* **2014**, *2*, 116108.
[20] R. Rice, J. Ballato, H. Injeyan, H. Komine, M. Wickham, US Patent 8934748, **2015**.
[21] C. Hou, X. Jia, L. Wei, S. Tan, X. Zhao, J. Joannopoulos, Y. Fink, *Nat. Commun.* **2015**, *6*, 6248.
[22] J. J. Kaufman, G. Tao, S. Shabahang, E. Banaei, D. S. Deng, X. Liang, S. Johnson, Y. Fink, A. F. Abouraddy, *Nature* **2012**, *487*, 463.
[23] A. Gumennik, L. Wei, G. Lestoquoy, A. M. Stolyarov, X. Jia, P. H. Rekemeyer, M. J. Smith, X. Liang, B. Grena, S. G. Johnson, S. Gradečak, A. F. Abouraddy, J. D. Joannopoulos, Y. Fink, *Nat. Commun.* **2013**, *4*, 2216.
[24] O. Aktas, E. Ozgur, O. Tobail, M. Kanik, E. Huseyinoglu, M. Bayindir, *Adv. Opt. Mater.* **2014**, *2*, 618.
[25] L. Rayleigh, *Proc. London Math. Soc.* **1878**, *10*, 4.
[26] L. Rayleigh, *Philos. Mag.* **1892**, *34*, 145.
[27] P. Patnaik, *Handbook of Inorganic Chemicals*, McGraw-Hill, New York, **2003**.
[28] T. Nishi, H. Shibata, H. Ohta, *Mater. Trans.* **2003**, *44*, 2369.
[29] S. Tomotika, *Proc. R. Soc. London, A* **1935**, *150*, 322.
[30] V. M. Glazov, S. N. Chizhevskaya, N. N. Glagoleva, *Liquid Semiconductors*, Plenum Press, New York **1969**.
[31] R. H. Doremus, *J. Appl. Phys.* **2002**, *92*, 7619.
[32] Y. Sato, T. Nishizuka, T. Tachikawa, M. Hoshi, T. Yamamura, Y. Waseda, *High Temp. - High Pressures* **2000**, *32*, 253.
[33] E. L. Dereniak, G. D. Boreman, *Infrared Detectors and Systems*, Wiley, New York **1996**.
[34] F. Sorin, G. Lestoquoy, S. Danto, J. D. Joannopoulos, Y. Fink, *Opt. Express* **2010**, *18*, 24264.
[35] T. Yin, R. Cohen, M. M. Morse, G. Sarid, Y. Chetrit, D. Rubin, M. J. Paniccia, *Opt. Express* **2007**, *15*, 13965.
[36] J. Liu, M. Beals, A. Pomerene, S. Bernardis, R. Sun, J. Cheng, L. C. Kimerling, J. Michel, *Nat. Photonics* **2008**, *2*, 433.
[37] D. Ritter, E. Zeldov, K. Weiser, *Phys. Rev. B* **1988**, *38*, 8296.
[38] F. Sorin, A. F. Abouraddy, N. Orf, O. Shapira, J. Viens, J. Arnold, J. D. Joannopoulos, Y. Fink, *Adv. Mater.* **2007**, *19*, 3872.
[39] K. Dreyer, F. R. Hickey, *Am. J. Phys.* **1991**, *59*, 619.
[40] S. Morris, T. Hawkins, P. Foy, C. McMillen, J. Fan, L. Zhu, R. Stolen, R. Rice, J. Ballato, *Opt. Mater. Express* **2011**, *1*, 1141.
[41] E. F. Nordstrand, A. N. Dibbs, A. J. Eraker, U. J. Gibson, *Opt. Mater. Express* **2013**, *3*, 651.
[42] F. Capasso, *Science* **1987**, *235*, 172.
[43] E. Ghahramani, J. E. Sipe, *Phys. Rev. B* **1989**, *40*, 12516.